Magnetic Resonance Image Restoration

Stephen J. Garnier
Griff L. Bilbro
James W. Gault
Wesley E. Snyder

Center for Communications and Signal Processing
Department of Electrical and Computer Engineering
North Carolina State University

TR-93/11
April 1993

Magnetic Resonance Image Restoration

Stephen J. Garnier and **Griff L. Bilbro**
Department of Electrical and Computer Engineering
North Carolina State University
Raleigh, NC 27695-7911

James W. Gault
U. S. Army Research Office
Research Triangle Park, NC

Wesley E. Snyder
Department of Radiology, Bowman-Gray School of Medicine
Wake Forest University, NC

ABSTRACT

We introduce a novel technique for Magnetic Resonance Image (MRI) restoration, using a physical model (spin equation) and corresponding basis images. We determine the basis images (proton density and nuclear relaxation times) from the MRI data and use them to obtain excellent restorations.

Magnetic Resonance Images depend nonlinearly on proton density, ρ, two nuclear relaxation times, T_1 and T_2, and two control parameters, TE and TR. We model images as Markov random fields and introduce two maximum *a posteriori* (MAP) restorations; quadratic smoothing and a nonlinear technique. We also introduce a novel method of global optimization necessary for the nonlinear technique.

1. INTRODUCTION

Magnetic Resonance Imaging (MRI) has proven to be a very useful noninvasive medical imaging method because of the ability to render high anatomical resolution of soft tissues.

Three variables form a basis for MR images: proton density, and two nuclear relaxation times. MRI systems can produce multiple images which emphasize one or several of these three basis variables while enforcing a reasonable level of registration between images, simply by adjusting one or more of the user-specified parameters, TE and TR.

At the present time, MR images are often processed or viewed individually, so some important clinical details may go unnoticed due to not using the joint information between multiple images. This problem can be avoided if an approach which incorporates multiple images is utilized, and done in a manner such that important basis images are extracted. Once this is done, synthetic images may be calculated from the basis images. These synthetic images can be used to generate images equivalent to data images obtainable with different control parameters, TE and TR, thereby minimizing the MR system time [17] [21] [5] .

In this work, the unknown basis images and the MR images are modeled as Markov random fields. The basis images are related to the MR images through a physical model. Two MAP restorations are compared; a simple quadratic smoothing prior and a nonlinear prior that is biased towards piecewise-smooth basis images. The application of the non-quadratic prior probabilities

requires global optimization, and here we present results of the nonlinear prior work. Our choice of nonlinear prior is based on our previous experience [2] with several approaches towards the nonlinear restoration of images. MR images synthesized by using the restored basis images are compared to the original MR data.

Section 2 discusses some existing techniques found in the literature. Section 3 presents useful information necessary for understanding our approach. In Section 4, the new contribution is discussed, and Section 5 reports experimental results.

2. BACKGROUND

The purpose of this section is to discuss the state of the art for the determination of the MRI basis images: proton density, and T_1 and T_2 nuclear relaxation times.

In MRI, typical images are proton density weighted images, T_1 weighted images, and T_2 weighted images, which are acquired through selection of appropriate values of TE and TR. At the present time, abnormal tissue areas are examined by the contrast in each image, and these images are viewed and treated separately by radiologists. Because of this single-image approach, MRI pulse sequences were developed to enhance the contrast of the characteristics of a particular tissue. However, through the utilization of routinely used "multi-echo" pulse sequences, several pixel-registered images can be obtained which reflect the different tissue properties. By analyzing these multiple pixel-registered images, the proton density, and the T_1 and T_2 nuclear relaxation times may be obtained for each sampled point in the multiple-image set.

Bobman, et al [4] [3] performed linear regression to obtain T_2 and pseudodensity, and separately used the same technique to calculate T_1, after which the calculated values were used to generate synthetic data. MacFall, Riederer and Wang [19] applied minimum-variance least-squares fitting to logarithmically processed data to calculate pseudodensity and T_2, and subsequently generated synthetic images. Breger, et al [6] used an iterative χ^2 minimization to produce pseudodensity and T_1 from four T_1 weighted images, and then used the same technique to calculate pseudodensity and T_2 from four T_2 weighted images. Lee and Riederer [16] used two images with constant TR and differing TE and directly calculated T_2 and pseudodensity, synthesized data using those values, and then evaluated the noise in the produced synthetics. Graumann, Fischer and Oppelt [11] designed a specific pulse sequence in order to directly calculate T_1 and T_2 without the use of minimization techniques. Wright, et al [22] discusses three algorithms for high-speed application. One algorithm uses an iteratively generated lookup table to map the quotient of two data points to T_1, and then determines the pseudodensity using back-substitution. The other algorithms were previously discussed [16] [19] . Brosnan, et al [7] discuss an improvement over Wiener filtering, "measurement-dependent filtering", which uses multiple data sources to decrease the noise in a previously calculated T_2 image while maintaining step edges. Liu, Nieminen and Koenig [18] use an unconstrained Newton-Raphson method with control parameters to iteratively calculate T_1. They separately calculate T_2 using a previously discussed [19] method, and then use the calculated T_1 and T_2 values to determine the spin density via back-substitution.

In all of the cited cases, the basis images have been calculated without the benefit of any *a priori* knowledge of the local characteristics of the tissues of interest. To date, only data images have been processed with the benefit of prior knowledge [10] [13] [9] [12] . It is our intent to use just such *a priori* knowledge to reduce the noise and increase the contrast within the basis images and subsequently synthesized restorations.

3. PROBLEM FORMULATION

The purpose of this section is to develop the definitions and mathematical basis for further discussion of our approach.

Let $\mathbf{G}$ be a measured vector-set of images

$$\mathbf{G} = \{\mathbf{g}_c\}_{c=1,d} \tag{1}$$

$$\mathbf{g}_c = [g_{c,i}]_{i=1,n}$$

where d is the number of channels in the vector-set, and where $g_{c,i}$ represents the c-th channel value associated with the i-th pixel.

Using similar notation, let $\mathbf{S}(\mathbf{F})$ represent the undegraded ideal images as a deterministic function of $\mathbf{F}$ where $\mathbf{F}$ are the undegraded ideal basis images, and let $\mathbf{N}$ represent additive noise such that $\mathbf{G} = \mathbf{S} + \mathbf{N}$. Note that

$$\mathbf{F} = \{\mathbf{f}_\psi\}_{\psi=1,p} \tag{2}$$

$$\mathbf{f}_\psi = [f_{\psi,i}]_{i=1,n}$$

where p is the number of basis images in the vector-set, and where $f_{\psi,i}$ represents the value associated with the i-th pixel of the ψ-th basis image.

3.1 Bayesian Model

Let $\hat{\mathbf{F}}$ be an estimate of $\mathbf{F}$. Bayes' rule gives the posterior distribution [8] of $\hat{\mathbf{F}}$ given the data $\mathbf{G}$ as

$$\mathrm{P}(\hat{\mathbf{F}}|\mathbf{G}) = \frac{\mathrm{P}(\mathbf{G}|\hat{\mathbf{F}})\mathrm{P}(\hat{\mathbf{F}})}{\mathrm{P}(\mathbf{G})} \,. \tag{3}$$

We refer to $\mathrm{P}(\mathbf{G}|\hat{\mathbf{F}})$ as the "noise term", and it describes the noise distribution. $\mathrm{P}(\hat{\mathbf{F}})$ is called the "prior term" and it describes the *a priori* distribution which can be chosen using *a priori* knowledge about $\mathbf{F}$. Obviously $\mathrm{P}(\mathbf{G})$ is constant and independent of $\hat{\mathbf{F}}$, so in order to maximize the posterior distribution, we need only maximize $\mathrm{P}(\mathbf{G}|\hat{\mathbf{F}})\mathrm{P}(\hat{\mathbf{F}})$.

The determination of the cost function, and the noise and prior terms of that cost function are presented in Section 4.

3.2 Physical Model

The function $\mathbf{S}(\mathbf{F})$ is given by the physical model. In this work, one simplified nonlinear image formation model [18] is used.

$$s_{c,i} = \rho_i \exp\left(-TE_c/T_{2i}\right)\left\{1 - \exp\left(-TR_c/T_{1i}\right)\right\} \tag{4}$$

where ρ, $\mathbf{T}_2$ and $\mathbf{T}_1$ are basis images of $\mathbf{f}_\psi$ where $\psi = 1, 2, 3$, respectively. T_1 and T_2 are nuclear relaxation times, and ρ represents proton density, contributions due to proton flow, and MRI system gain. Most brain tissue is perfuse with slowly moving blood, hence the data should not be subject to large variations in proton flow. This work does not address the effect of proton flow. Our data was acquired with MRI system gain held constant for all scans.

Note that this physical model is undefined and exhibits singularities in the gradient when T_1 or T_2 equals zero. Because of this, a constrained optimization technique is required to find a global solution in the minimization process.

4. IMAGE RESTORATION

This section delineates the different approaches we have taken towards restoration of the basis images through deterministic minimization of a cost function. In all cases, a maximum likelihood ("noise") term is necessary to ensure fidelity to the data. A "prior" term is introduced into the minimization scheme only when neighborhood interactions are necessary to correct the effects of noise-corrupted data. This noise propagates in a nonlinear and signal-dependent manner [19] [1] into the basis images described within the physical model. The "prior" term addresses this effect by operating on the basis images within a local neighborhood.

4.1 The Noise Term, H_N

The maximum likelihood approach does not incorporate a prior model, hence the restoration is based solely on a noise term. For the maximum likelihood case, the noise which has corrupted $\mathbf{S(F)}$ is modeled as stationary, signal-independent additive Gaussian noise [19] , hence $\mathrm{P}(\mathbf{G}|\hat{\mathbf{F}})$ is given by

$$\mathrm{P}(\mathbf{G}|\hat{\mathbf{F}}) = \mathrm{P}(\mathbf{N}) \equiv \frac{\exp\left(-\frac{1}{2}\mathbf{N}^{\mathrm{t}}\mathbf{C}^{-1}\mathbf{N}\right)}{(2\pi)^{nd/2}|\mathbf{C}|^{1/2}} \tag{5}$$

where $\mathbf{C}$ denotes the covariance matrix of noise $\mathbf{N}$, and $|\mathbf{C}|$ denotes the determinant of $\mathbf{C}$. Since the noise is assumed to be zero-mean, $\mathbf{C} = \mathbf{R}$, the autocorrelation matrix, and Equation 5 can now be written as

$$\mathrm{P}(\mathbf{G}|\hat{\mathbf{F}}) = \frac{\exp\left(-\frac{1}{2}(\hat{\mathbf{S}}(\hat{\mathbf{F}}) - \mathbf{G})^{\mathrm{t}}\mathbf{R}^{-1}(\hat{\mathbf{S}}(\hat{\mathbf{F}}) - \mathbf{G})\right)}{(2\pi)^{nd/2}|\mathbf{R}|^{1/2}} = \tag{6}$$

$$\exp\left(K - \frac{1}{2}(\hat{\mathbf{S}}(\hat{\mathbf{F}}) - \mathbf{G})^{\mathrm{t}}\mathbf{R}^{-1}(\hat{\mathbf{S}}(\hat{\mathbf{F}}) - \mathbf{G})\right)$$

where K is some constant value. Taking the negative-log of $\mathrm{P}(\mathbf{G}|\hat{\mathbf{F}})$, and harmlessly ignoring the constant contribution of K, the "noise term" of the optimization function is obtained:

$$H_N(\hat{\mathbf{F}}, \mathbf{G}) = \frac{1}{2}(\hat{\mathbf{S}}(\hat{\mathbf{F}}) - \mathbf{G})^{\mathrm{t}}\mathbf{R}^{-1}(\hat{\mathbf{S}}(\hat{\mathbf{F}}) - \mathbf{G}) = \tag{7}$$

$$\sum_c \frac{1}{2{\sigma_c}^2} \sum_i \left(\hat{s}_{c,i}(\hat{\mathbf{F}}) - g_{c,i}\right)^2,$$

for isotropic uncorrelated noise.

In order to ascertain the maximum likelihood ρ, T_2 and T_1 images, we arbitrarily set the initial basis images to the following values:

$$T_{1_i} = \frac{1}{N}\sum_{c=0}^{N-1} TR_c \tag{8}$$

$$T_{2_i} = \frac{1}{N}\sum_{c=0}^{N-1} TE_c \tag{9}$$

$$\rho_i = \frac{1}{N}\sum_{c=0}^{N-1} g_{c,i} \exp\left(TE_c/T_{2_i}\right)\left\{1 - \exp\left(-TR_c/T_{1_i}\right)\right\}^{-1} \tag{10}$$

For the case where only maximum likelihood restoration is attempted, the cost function is $H = H_N$.

4.2 The Quadratic Prior Term, H_P

Smoothing requires the use of an additional term in the cost function, the prior term. This term, $\mathrm{P}(\hat{\mathbf{F}})$, depends only on $\hat{\mathbf{F}}$, and should reflect some prior knowledge of the nature of $\mathbf{F}$. For the case of MR images, the basis images should appear to be locally homogeneous in some important way.

Since it is frequently used in similar restoration problems [8], an exponential form is chosen for $\mathrm{P}(\hat{\mathbf{F}})$:

$$\mathrm{P}(\hat{\mathbf{F}}) = \frac{\exp\left(-H_p(\hat{\mathbf{F}})\right)}{Z_p} \tag{11}$$

where Z_p normalizes $\mathrm{P}(\hat{\mathbf{F}})$. $H_p(\hat{\mathbf{F}})$ in this instance is used to measure and regulate the local homogeneity of some characteristic of the basis images.

For the case of quadratic smoothing, we choose

$$H_p(\hat{\mathbf{F}}) = \lambda \sum_{\psi} \frac{1}{2{\sigma_\psi}^2} \sum_{i} \sum_{\eta} w_\eta \left(\frac{\partial \hat{f}_{\psi,i}}{\partial x_\eta} \right)^2 \tag{12}$$

where η indicates the direction of the first-order partial differential, w_η adjusts the relative contribution of nearest-neighbor versus next-nearest-neighbor pixels, and λ, in conjunction with the estimate of noise in the ψ-th image, σ_ψ, indicates the emphasis of smoothing on the basis images.

To determine the smoothed values for the ρ, T_2 and T_1 images, we initialize these values with the method put forth in Equations 8, 9 and 10. When neighborhood interactions are used, the cost function is written as $H = H_N + H_P$.

4.2 The Nonlinear Prior Term, H_P

Quadratic smoothing performs well in regions where the basis images do not exhibit large excursions or contain step edges. In areas where the maximum likelihood solution yields such large excursions, quadratic smoothing heavily blurs these features. The advantage of nonlinear smoothing is that it can preserve these features while maintaining the same level of smoothing performance on those regions where large excursions do not exist.

For the case where nonlinear piecewise smoothing is desirable,

$$H_p(\hat{\mathbf{F}}) = \lambda \sum_{\psi} \sum_{i} \frac{\sum_\eta w_\eta \left(\frac{\partial f_{\psi,i}}{\partial x_\eta} \right)^2}{2{\sigma_\psi}^2 + \frac{1}{{\tau_\psi}^2} \sum_\eta w_\eta \left(\frac{\partial f_{\psi,i}}{\partial x_\eta} \right)^2} \tag{13}$$

where λ is a constant and τ_ψ is a smoothly changing annealing parameter on the ψ-th basis image. At infinite τ_ψ for all ψ, the prior term is equivalent to the previously discussed quadratic prior term. As τ_ψ is decreased, the influence of the prior term gives way to the noise term, and the restoration takes on the appearance of the maximum likelihood solution as $\tau_\psi \to 0$. For the maximum likelihood case, the solution for reasonable SNR is obtained within a system with a single local minimum. For the quadratic smoothing case, the prior term is convex. Figure 1 illustrates the nonlinear prior function at several temperatures for the function $x^2/(1 + \frac{x^2}{\tau^2})$.

For the case of nonlinear restoration, we initialize the basis images with the output from the quadratic smoothing case. τ_ψ must be initially set to a value high enough to ensure that the interim

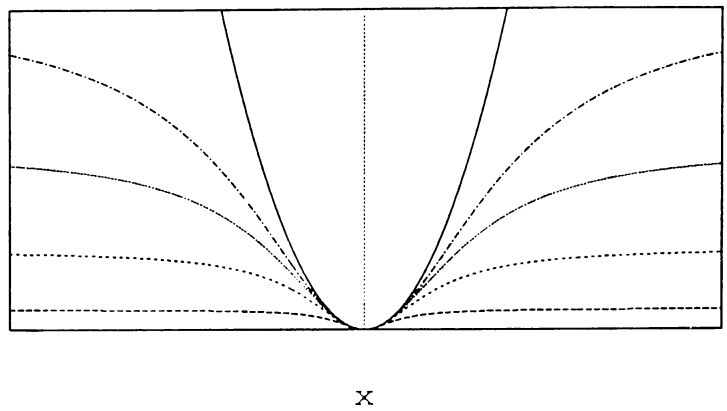

Figure 1: The nonlinear prior function at several temperatures.

restoration for those τ_ψ closely approximates the final restoration for quadratic smoothing. Once the minimum has been obtained for that initial temperature, τ_ψ is reduced by a small amount, and a minimum is again sought. This continues until an acceptable restoration is obtained. By choosing a reasonable annealing schedule, these final τ_ψ values produce a piecewise smooth restoration between the quadratically smoothed and maximum likelihood solutions; that is, a restoration that is both locally smooth and yet retains fidelity to the data by preserving step edges. In this way, we start from an overly smoothed restoration, and anneal to a final restoration which does not overly suppress single-pixel disturbances which a radiologist might find important.

5. EXPERIMENTAL RESULTS

Figures 2 through 9 are of a subject's brain. The three data images presented within Figures 2 through 4 were obtained by two scanning sequences of a presumably healthy subject. The control parameters were set at (TE,TR) = (30,900), (90,900) and (90,1800), respectively. It should be noted that a total of four immediately-adjacent 3 millimeter slices were acquired, and that the three data images presented here are common to only one of those slices. Typical clinical slice thicknesses are 5 to 6 millimeters.

5.1 Restorations

Figures 2 through 4 are original MRI data. No maximum likelihood restorations are presented here, since the pixels of basis images extracted from valid data coincide exactly with the data (three equations and three unknowns). Figures 5 and 6 illustrate the quadratically smoothed and nonlinearly smoothed restorations, respectively. Due to the dynamic ranges involved, it is not possible to display all five figures videoscaled to a common scale. However, the restorations in Figures 5 and 6, and the data in Figure 3 can be directly compared since they use a common scale. In all cases, the restorations produced from the nonlinearly smoothed basis images are visually superior in noise reduction and edge preservation to those provided by both the maximum likelihood and quadratically smoothed basis images.

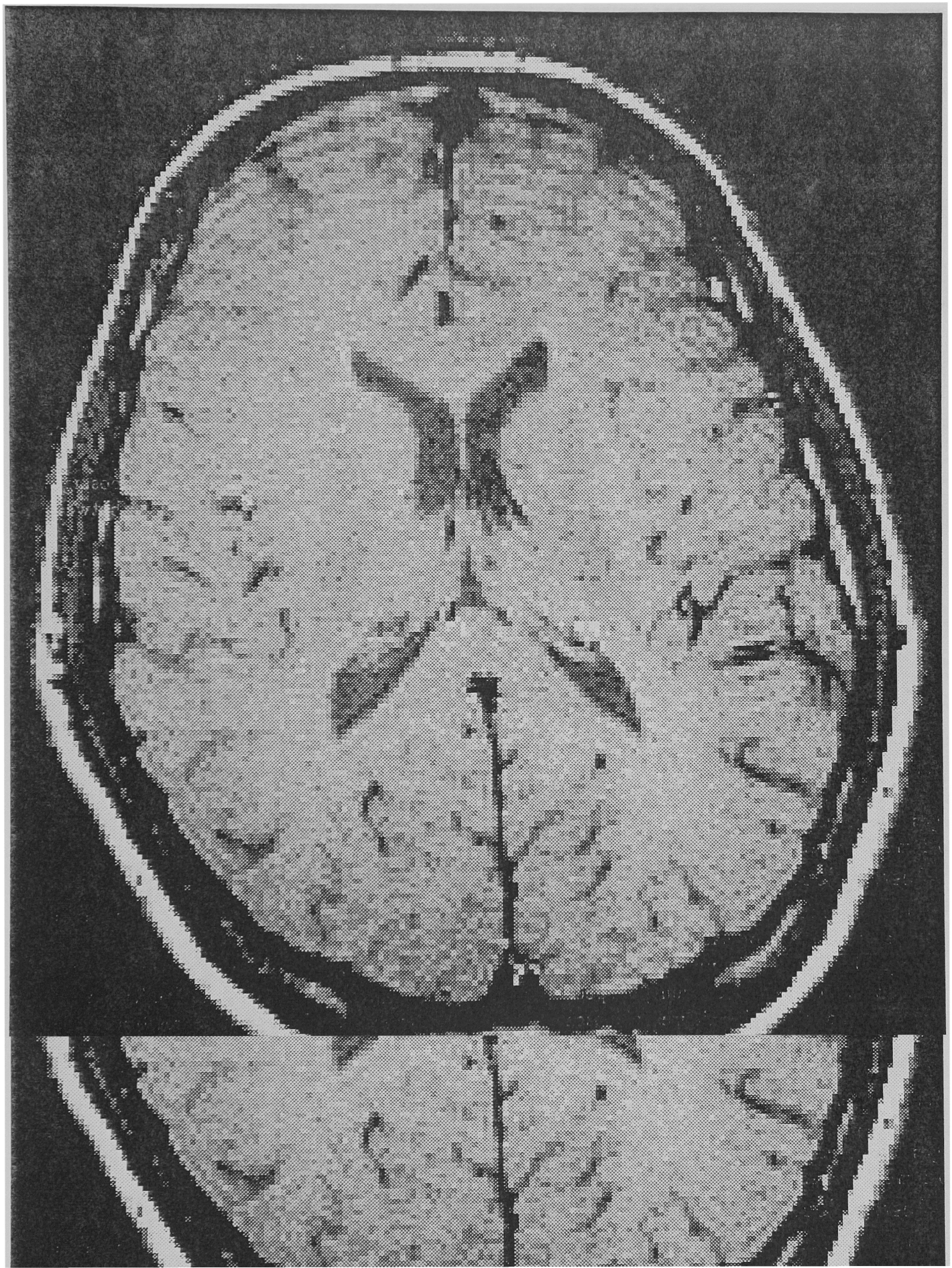

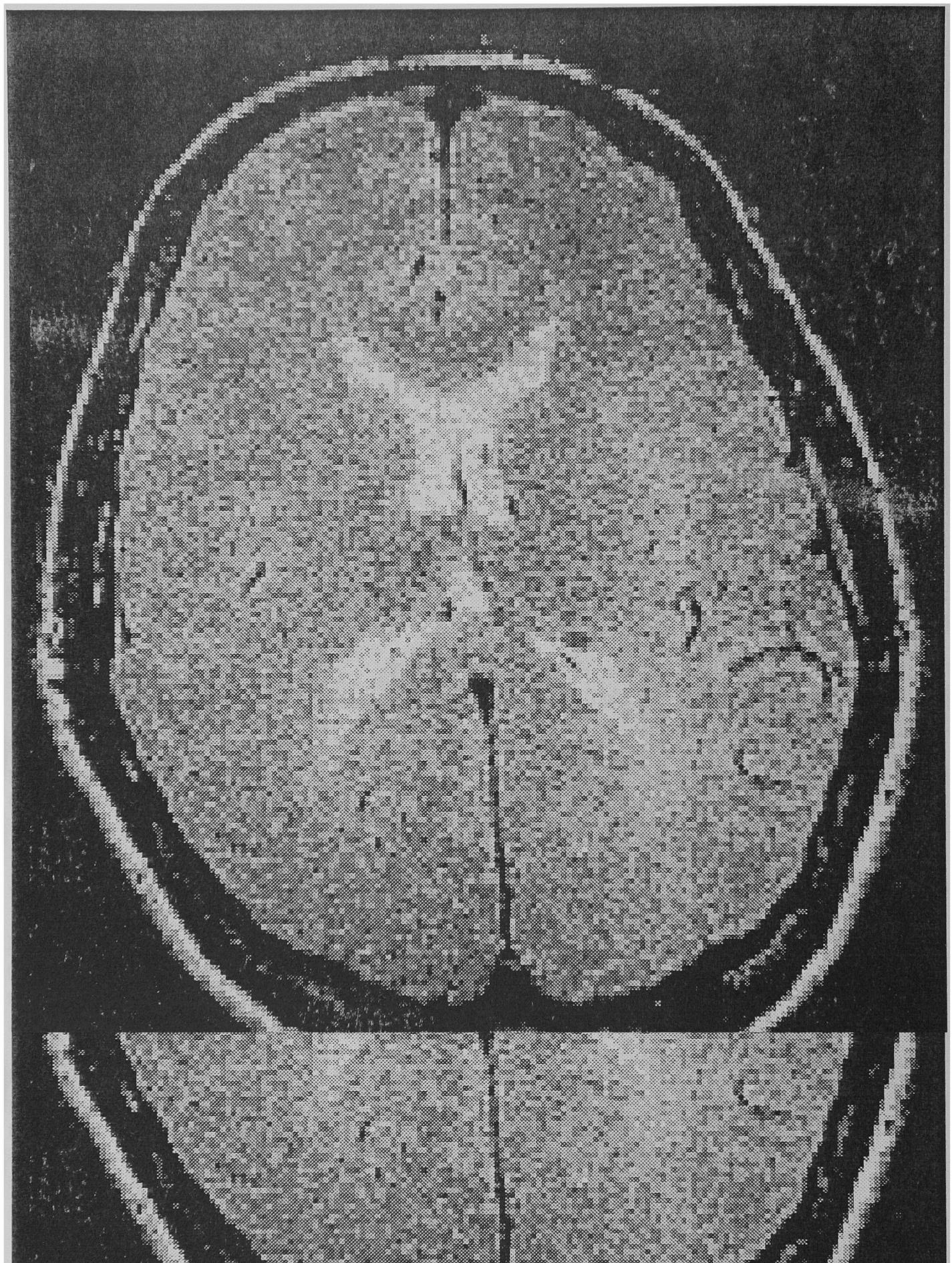

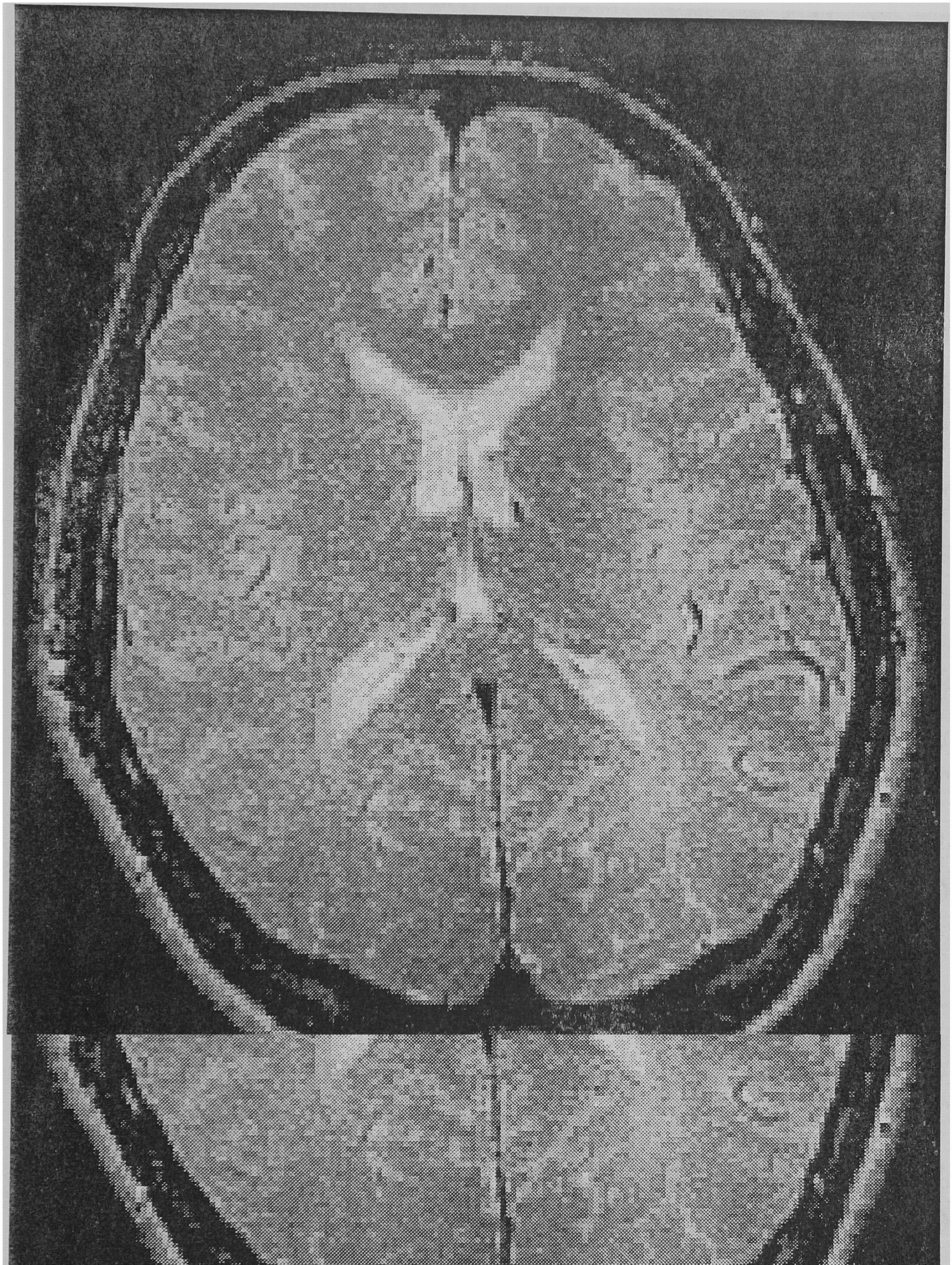

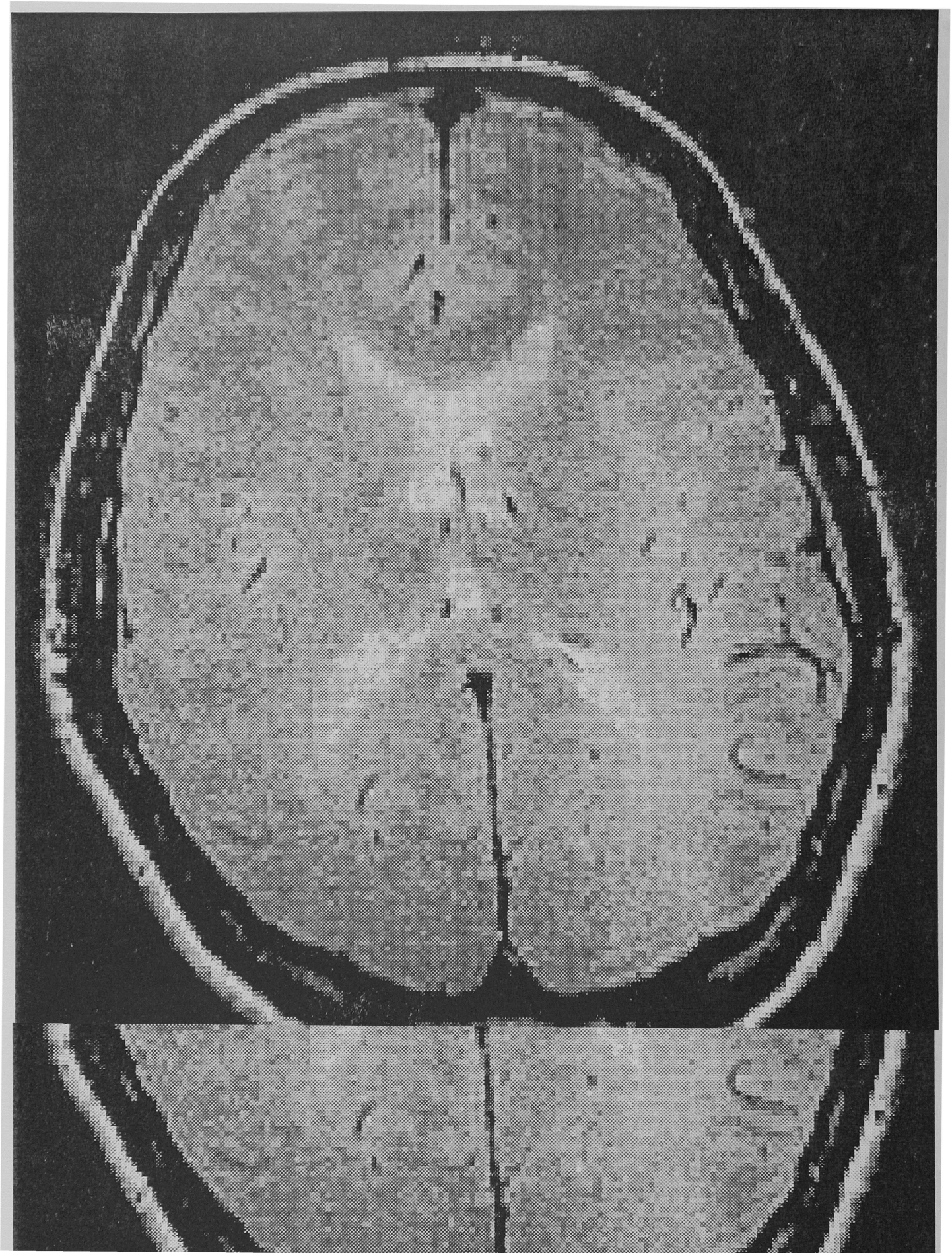

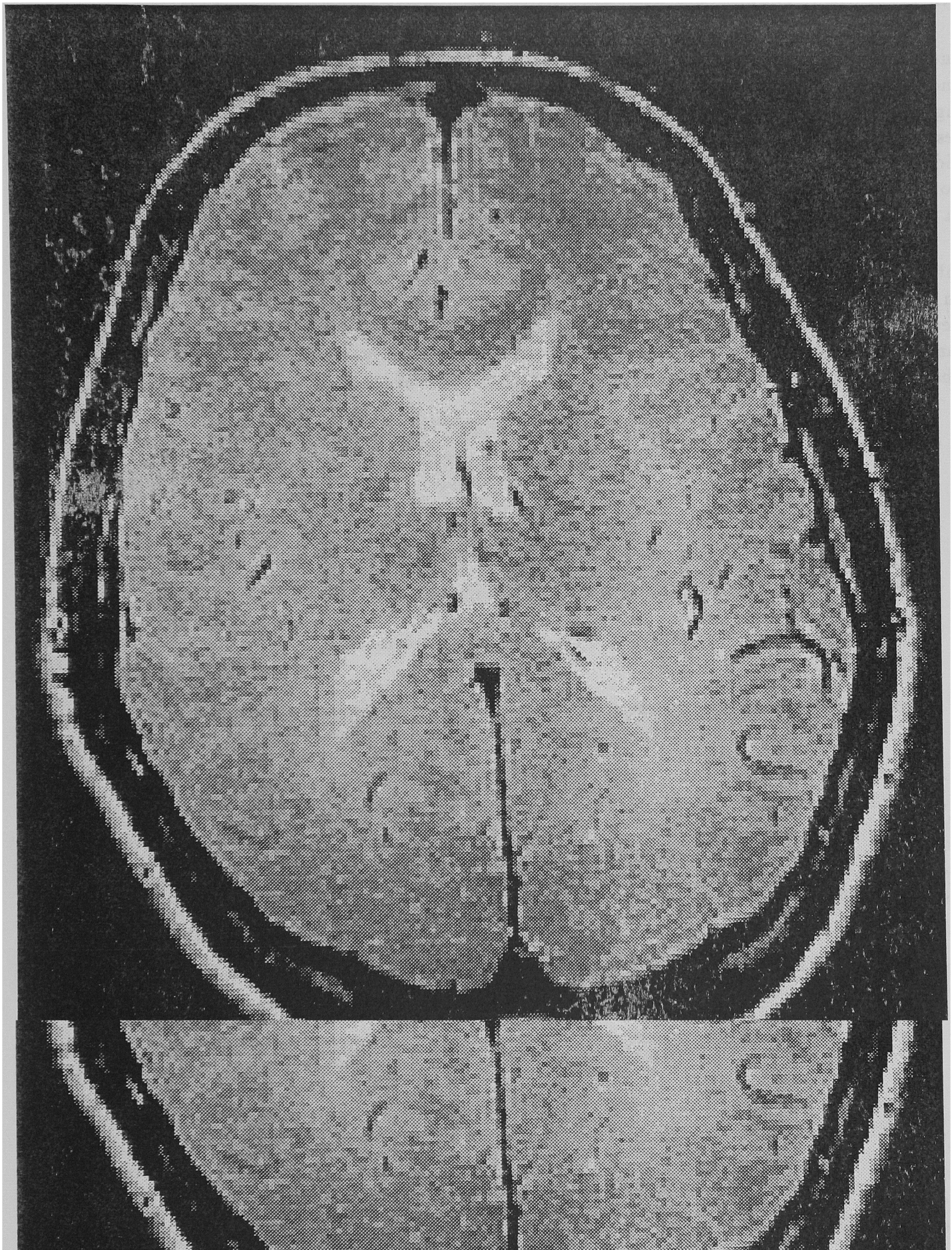

5.2 Estimated Basis Images

The basis images are of interest since the proposed method uses a physical model (Equation 4) and corresponding control parameters. Figures 7, 8 and 9 are extracted from the area surrounding and including the CSF-filled ventricles of the subject's brain. All of these figures have the following images placed left to right: the maximum likelihood restoration, the quadratically smoothed restoration, and the nonlinearly smoothed restoration. All images within a single figure have been videoscaled to a common scale. Due to the dynamic range in the maximum likelihood images, it is not possible to display all the restorations to a common scale without truncating the many outliers in the maximum likelihood restorations. These truncated pixel values are illustrated as white.

We note that the many outliers in the maximum likelihood images are likely due to "interslice interference" [15] [14] [20] , since the data was acquired without any distance between adjacent slices. In this case, the calculated T_1 relaxation time has likely been heavily influenced by cross-excitation between adjacent slices. As can be seen in Equation 4, the calculated density also suffers, since a large error in the determination of T_1 directly impacts on the estimate of ρ. This is supported by observing the maximum likelihood images in Figures 7 and 9.

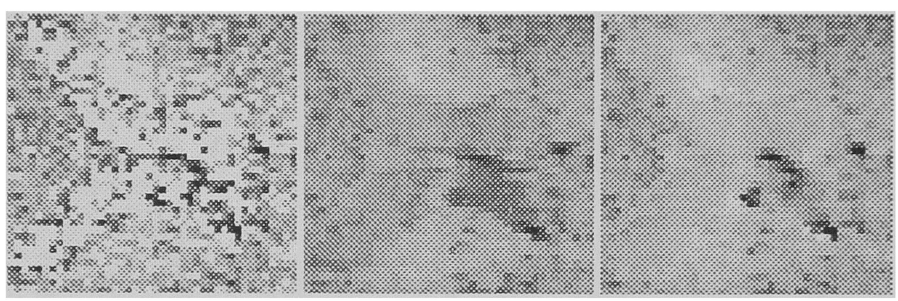

Figure 7: Proton Density Restorations.

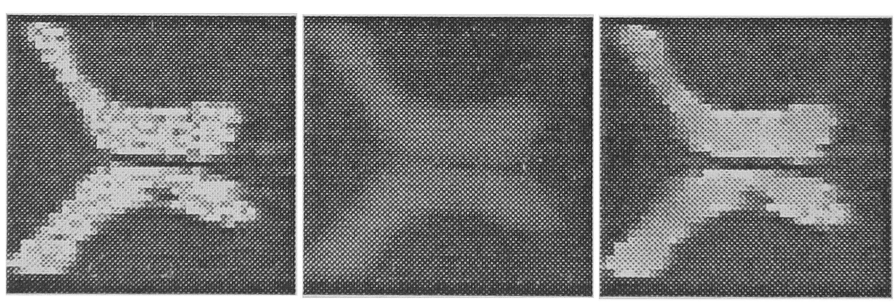

Figure 8: T_2 restorations.

6. CONCLUSION

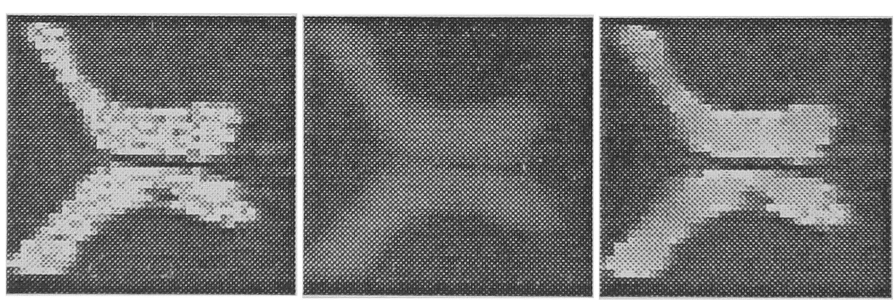

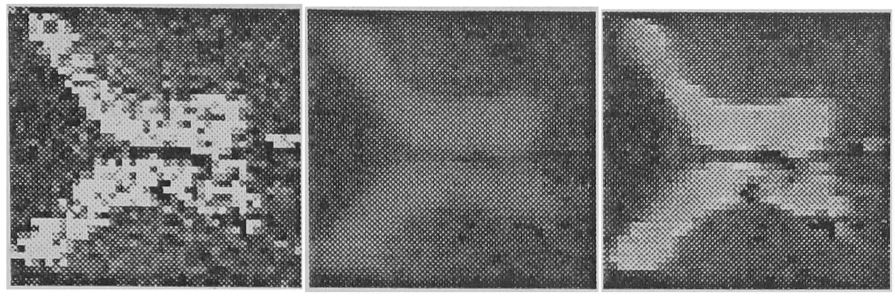

Figure 9: T_1 restorations.

based on *a priori* knowledge of the local characteristics of the tissues of interest, which allows us to reduce noise in the basis images while preserving step edges and other single pixel excursions which a radiologist might find important. Furthermore, we have shown that the restorations generated from these nonlinearly-smoothed basis images are visually superior in noise reduction and edge preservation to those provided by both the maximum likelihood and quadratically-smoothed basis images. It is in this manner that we have developed a method which obtains images which most clearly differentiate soft tissue types in MRI data.

7. ACKNOWLEDGEMENTS

This work was supported by the U. S. Army Research Office under Contract DAAL03-89-D-0003-0004 and by the Center for Communications and Signal Processing, North Carolina State University. We would also like to express our gratitude to W. H. Hinson at the Bowman-Gray School of Medicine, Wake Forest University, for providing data images and technical assistance.

References

[1] C. J. G. Bakker and C. N. De Graff. Precision in calculated ρ, T_1 and T_2 images as a function of data analysis method. *Magnetic Resonance Imaging*, 6:3–8, 1988.

[2] G. L. Bilbro, W. E. Snyder, S. J. Garnier, and J. W. Gault. Mean field annealing: A formalism for constructing GNC-like algorithms. *IEEE Transactions on Neural Networks*, 3(1):131–138, January 1992.

[3] S. A. Bobman, S. J. Riederer, J. N. Lee, S. A. Suddarth, H. Z. Wang, B. P. Drayer, and J. R. MacFall. Cerebral magnetic resonance image synthesis. *American Journal of Neuroradiology*, 6:265–269, March/April 1985.

[4] S. A. Bobman, S. J. Riederer, J. N. Lee, S. A. Suddarth, H. Z. Wang, and J. R. MacFall. Synthesized MR images: Comparison with acquired images. *Radiology*, 155(3):731–738, 1985.

[1] C. J. G. Bakker and C. N. De Graff. Precision in calculated ρ, T_1 and T_2 images as a function of data analysis method. *Magnetic Resonance Imaging*, 6:3–8, 1988.

[2] G. L. Bilbro, W. E. Snyder, S. J. Garnier, and J. W. Gault. Mean field annealing: A formalism for constructing GNC-like algorithms. *IEEE Transactions on Neural Networks*, 3(1):131–138, January 1992.

[3] S. A. Bobman, S. J. Riederer, J. N. Lee, S. A. Suddarth, H. Z. Wang, B. P. Drayer, and J. R. MacFall. Cerebral magnetic resonance image synthesis. *American Journal of Neuroradiology*,

[7] T. Brosnan, G. Wright, D. Nishimura, Q. Cao, A. Macovski, and F. G. Sommer. Noise reduction in magnetic resonance imaging. *Magnetic Resonance in Medicine*, 8:394–409, 1988.

[8] D. Geman and S. Geman. Stochastic relaxation, Gibbs distributions, and the Bayesian restoration of images. *IEEE Transactions on Pattern Analysis and Machine Intelligence*, PAMI-6(6):721–741, November 1984.

[9] G. Gerig, O. Kuebler, R. Kikinis, and F. A. Jolesz. Nonlinear anisotropic filtering of mri data. *IEEE Transactions on Medical Imaging*, 1992.

[10] F. Godtliebsen. Noise reduction using markov random field. *Journal of Magnetic Resonance*, 92:102–114, 1991.

[11] R. Graumann, H. Fischer, and A. Oppelt. A new pulse sequence for determining T_1 and T_2 simultaneously. *Medical Physics*, 13(5):644–647, September/October 1986.

[12] Y. S. Han and W. E. Snyder. Multi-variate MR image restoration using vector mean field annealing. In *SPIE Proceedings Volume 1768: Mathematical Methods in Medical Imaging, 1992*, San Diego, California, July 1992. SPIE's 1992 International Symposium on Optical Applied Science and Engineering.

[13] X. Hu, V. Johnson, W. Wong, and C. Chen. Bayesian image processing in magnetic resonance imaging. *Magnetic Resonance Imaging*, 9:611–620, 1991.

[14] M. Just, H. P. Higer, and P. Pfannenstiel. Errors in T_1-determination using multislice technique and Gaussian slice profiles. *Magnetic Resonance Imaging*, 6:53–56, 1988.

[15] J. B. Kneeland, A. Shimakawa, and F. W. Wehrli. Effect of intersection spacing on MR image contrast and study time. *Radiology*, 158:819–822, 1986.

[16] J. N. Lee and S. J. Riederer. Optimum acquisition times of two spin echoes for MR image synthesis. *Magnetic Resonance in Medicine*, 3:634–638, 1986.

[17] J. N. Lee, S. J. Riederer, S. A. Bobman, F. Farzaneh, and H. Z. Wang. Instrumentation for rapid MR image synthesis. *Magnetic Resonance in Medicine*, 3:33–43, 1986.

[18] J. Liu, A. O. K. Nieminen, and J. L. Koenig. Calculation of T_1, T_2, and proton spin density images in nuclear magnetic resonance imaging. *Journal of Magnetic Resonance*, 85:95–110, 1989.

[19] J. R. MacFall, S. J. Riederer, and H. Z. Wang. An analysis of noise propogation in computed T_2, pseudodensity, and synthetic spin-echo images. *Medical Physics*, 13(3):285–292, May/June 1986.

[20] S. Majumdar, H. D. Sostman, and J. R. MacFall. Contrast and accuracy of relaxation time measurements in acquired and synthesized multislice magnetic resonance images. *Investigative Radiology*, 24(2):119–127, February 1989.

[21] D. A. Ortendahl, N. M. Hylton, L. Kaufman, J. C. Watts, L. E. Crooks, C. M. Mills, and D. D. Stark. Analytical tools for magnetic resonance imaging. *Radiology*, 153(2):479–488, 1984.

[22] R. C. Wright, S. J. Riederer, J. N. Lee, F. Farzaneh, and J. B. De Castro. High-speed techniques for estimating T_1, T_2, and density images. *IEEE Transactions on Medical Imaging*, MI-6(2):165–168, June 1987.